Bioinformatics analysis of PSAT1 loss identifies downstream pathways regulated in EGFR mutant NSCLC and a selective gene signature for predicting the risk of relapse

RUMEYSA BIYIK-SIT[1,2], SABINE WAIGEL[2,3], KALINA ANDREEVA[3,4], ERIC ROUCHKA[1,3] and BRIAN F. CLEM[1,2]

[1]Department of Biochemistry and Molecular Genetics, University of Louisville, Louisville, KY 40202, USA; [2]Brown Cancer Center, Louisville, KY 40202, USA; [3]Kentucky IDeA Network of Biomedical Research Excellence Bioinformatics Core, University of Louisville, Louisville, KY 40202, USA; [4]Department of Neuroscience Training, University of Louisville, Louisville, KY 40202, USA

Received June 23, 2024; Accepted September 25, 2024

DOI: 10.3892/ol.2024.14755

Abstract. The majority of malignant tumors exhibit an altered metabolic phenotype that ultimately provides the required energy and molecular precursors necessary for unregulated cell division. Within this, phosphoserine aminotransferase 1 (PSAT1) is involved in *de novo* serine biosynthesis and its activity promotes various biochemical processes, including one-carbon metabolism. It also directly generates α-ketoglutarate (α-KG), a Kreb cycle intermediate and epigenetic-regulating metabolite. Prior studies examining PSAT1 depletion have identified individual affected downstream pathways, such as GSK3β and E2F, in several cancer types, including non-small-cell lung cancer (NSCLC). However, global gene expression examination in response to PSAT1 loss, particularly in EGFR mutant NSCLC, has not been unexplored. Transcriptional profiling of EGFR mutant NSCLC cells with or without stable knock-down of PSAT1 identified differentially expressed genes (DEGs) enriched in several metabolic pathways required for cell division, including amino acid and nucleotide biosynthesis. Supplementation studies involving non-essential amino acids, nucleosides and α-KG partially restored defects in anchorage-independent growth due to the knockdown of PSAT1. Kyoto Encyclopedia of Genes and Genomes and Gene Ontology enrichment analysis identified potential impacts on actin cytoskeleton arrangement and β-catenin activity, which were rescued by PSAT1 re-expression. Finally, a comparative analysis of PSAT1 DEGs against transcripts enriched in patient EGFR mutant lung tumors identified a gene signature that is associated with overall and relapse-free survival (RFS) and was able to distinguish low or high-risk populations for RFS in early-stage EGFR mutant NSCLC. Overall, investigating genes altered by PSAT1 loss confirmed known PSAT1-regulated cellular pathways, identified a previously unknown role in the mediation of cytoskeleton arrangement in EGFR mutant NSCLC cells and allowed for the characterization of a gene signature with putative predictive potential for RFS in early-stage disease.

Correspondence to: Dr Brian F. Clem, Department of Biochemistry and Molecular Genetics, University of Louisville, 505 South Hancock Street, Louisville, KY 40202, USA
E-mail: brian.clem@louisville.edu

Abbreviations: α-KG, α-ketoglutarate; AUC, area under the curve; DEG, differentially expressed gene; EGFR, epidermal growth factor receptor; KM, Kaplan Meier; NEAA, non-essential amino acids; NSCLC, non-small cell lung cancer; OS, overall survival; PHGDH, phosphoglycerate dehydrogenase; PKM2, pyruvate kinase M2; PSAT1, phosphoserine aminotransferase 1; PSPH, phosphoserine phosphatase; RFS, relapse-free survival; SSP, serine synthesis pathway; TKI, tyrosine kinase inhibitor

Key words: EGFR mutant, NSCLC, bioinformatics, metabolism, PSAT1

Introduction

Metabolic rewiring in support of the energetic and biosynthetic needs required for untethered cell proliferation is a hallmark observed in the majority of human cancers (1). This encompasses not only changes in glycolytic metabolism but alterations in fatty acid synthesis/oxidation and amino acid utilization. Recently, activity within the *de novo* serine synthesis pathway (SSP) has been observed to be elevated in several tumor types, including NSCLC (2-4). The SSP originates from the glycolytic intermediate, 3-phosphoglycerate, which is converted to serine through enzymatic activities of phosphoglycerate dehydrogenase (PHGDH), phosphoserine aminotransferase (PSAT1), and phosphoserine phosphatase (PSPH). Serine can then be utilized in protein synthesis and as one-carbon units for the folate and methionine cycles. Interestingly, serine is a non-essential amino acid (NEAA) that can be imported from the extracellular space. Metabolism through the SSP also generates NADH and α-ketoglutarate (α-KG), the latter of which is a key Kreb cycle intermediate and epigenetic regulator important for tumorigenic growth. Further, manipulation of SSP enzymes has been previously demonstrated to alter cell proliferation and migration/invasion in multiple cancer cell types both *in vitro* and *in vivo* (5-7).

PSAT1 catalyzes the interconversion of phosphohydroxypyruvate and glutamate to phosphoserine and α-KG. Genetic knockdown studies have identified a requirement for PSAT1 in ovarian, colorectal, glioblastoma, and subtypes of both NSCLC and breast cancer (8-11). Loss of PSAT1 not only suppresses cell proliferation and metastatic potential but also promotes chemosensitivity to several clinically used agents, such as platinum-based chemotherapies and TKIs (12,13). Functional analysis has identified multiple cellular effectors affected by PSAT1 suppression, including E2F-CyclinD1 and β-catenin (7,14,15). However, a broad analysis of gene expression changes in response to PSAT1 manipulation has not been examined, particularly in the context of NSCLC.

Disruption of key metabolic mediators not only hampers nutrient utilization but can also lead to specific transcriptional changes (16,17). Transcriptomic profiling, such as RNA-seq, under these conditions, allows the interrogation of genome-wide changes controlled by these metabolic activities. Bioinformatics analysis of these datasets can then identify impacted pathways or altered cellular processes, which can be further extended to define expression differences between patient cohorts with respect to tumor staging, response to therapy, and/or survival outcomes (18-20). In our previous study, it was demonstrated that EGFR activation promoted PSAT1 nuclear translocation, which was required for proper nuclear localization of pyruvate kinase M2 (PKM2) (11). It was thus hypothesized that PSAT1 loss may yield a robust transcriptional response due to this selective compartmentalization and the known transcriptional activity of PKM2 (16). Given this specific signal-dependent nuclear trafficking, the cellular response to PSAT1 knockdown in EGFR mutant NSCLC was examined here. Transcriptomic analysis detailed multiple affected pathways, such as actin-cytoskeleton arrangement and β-catenin activity, which were functionally verified in EGFR mutant NSCLC cells. In addition, a comparative analysis of these differentially expressed genes with transcriptomic changes observed in EGFR mutant NSCLC patient tumors identified a gene signature with prognostic potential for RFS that was able to distinguish high-risk patients with stage 1 disease.

Materials and methods

Reagents and antibodies. Antibodies against PKM2 (cat. no. 4053), β-catenin (cat. no. 8480), OCT1 (cat. no. 8157), and α-tubulin (cat. no. 3873) were obtained from Cell Signaling Technology, Inc. The anti-PSAT1 (cat. no. 10501-1-AP) antibody was purchased from ProteinTech Group, Inc. β-actin (cat. no. A2228), 100x EmbryoMax Nucleosides (cat. no. ES-008-D), and Dimethyl 2-oxoglutarate (cat. no. 349631) were obtained from MilliporeSigma. pGL4.49[luc2P/TCF-LEF/Hygro] Vector (E4611) and the Dual-Luciferase Reporter Assay System (cat. no. E1960) were purchased from Promega Corporation. Difco Noble Agar (cat. no. 214220) was purchased from BD Biosciences and 100x NEAA (cat. no. 25-025) was obtained from Corning Inc.

Cell culture. Generation of stably transfected PC9 cells (Control and shPSAT1 PC9, Control-EV, shPSAT1-EV, shPSAT1-FLAG-PSAT1, and shPSAT1-PKM2$^{NLS\text{-}K433Q}$) were established from parental PC9 cells provided by Dr Levi Beverly (University of Louisville) after STR profiling, as described previously (11). The PSAT1 shRNA (TRCN0000291729: target sequence: GCACTCAGTGTT GTTAGAGAT; pLKO-puro plasmid backbone) and the pLKO-puro non-mammalian shRNA control (SHC202: CCG GCAACAAGATGAAGAGCACCAACTCGAGTTGGTGCT CTTCATCTTGTTGTTTTT) plasmids used to establish the shPSAT1 and Control PC9 cells, respectively, were purchased from Millipore Sigma. Control and shPSAT1 PC9 cells were maintained in RPMI media (Gibco) supplemented with 10% FBS, 50 μg/ml gentamicin (Gibco; Thermo Fisher Scientific, Inc.), and 1 μg/ml puromycin (Gibco; Thermo Fisher Scientific, Inc.). Control-EV, shPSAT1-EV, shPSAT1-FLAG-PSAT1, and shPSAT1-PKM2$^{NLS\text{-}K433Q}$ PC9 cells were maintained in RPMI media (Gibco; Thermo Fisher Scientific, Inc.) supplemented with 10% FBS, 50 μg/ml gentamicin (Gibco; Thermo Fisher Scientific, Inc.), 1 μg/ml puromycin, and 200 μg/ml geneticin (Gibco; Thermo Fisher Scientific, Inc.). InvivoGen Mycostrips (rep-mys-50) were used to continuously assess for mycoplasma contamination, and all cells were cultured in humidified incubators at 37˚C and 5% CO_2.

RNA-seq transcriptomic profiling and analysis

Data acquisition and pre-processing. A total of three distinct sets of RNA for RNA-seq profiling were prepared from 24-h serum-starved Control and shPSAT1 PC9 cells. Samples were submitted to the University of Louisville Genomics Facility, which performed the library preparation and sequencing reactions. Sequencing was performed on an Illumina NextSeq 500 Platform using the High Output Kit v2 with 75 cycles (cat. no. FC-40402005, Illumina, Inc.). Sequencing data has been submitted to the Gene Expression Omnibus (GEO; accession no. GSE173270). The KYINBRE Bioinformatics core was used to perform the initial data analysis. Raw fastq files were mapped to the human hg38 reference genome using tophat2 (version 2.0.13) (21). Differentially expressed genes were determined for each pairwise comparison using the tuxedo suite (cufflinks-cuffdiff2) (version 2.2.1) (22) with Ensembl v82 annotations. Normalized Fragments Per Kilobase of transcript per Million mapped reads (FPKM) expression values and statistical analysis results from cuffdiff2, including P- and q-value with ENSEMBL gene ID, were downloaded for further investigation.

Identification of differentially expressed genes (DEGs). The following parameters served as the selection criterion for DEGs: the absolute value of $\log_2$(shPSAT1/Control) ≥0.48, FPKM value (Control or shPSAT1) ≥5, and q-value ≤0.05. Genes were divided into two groups, down-regulated genes (termed shPSAT1-down-regulated) and up-regulated genes (termed shPSAT1-up-regulated), based on the comparison between shPSAT1 and control PC9 cells. For hierarchical cluster analysis, the normalized log-transformed expression txt files were imported to Cluster 3 software and clustered based on the average linkage (23). The output was visualized using Java Treeview software (24).

Functional analysis. Functional and KEGG pathway analyses were conducted by uploading the ENSEMBL IDs to MSigDB version 7.4 (https://www.gsea-msigdb.org/gsea/msigdb). The top 20 enriched pathways and datasets for KEGG pathways,

chemically and genetically perturbed data sets (CGP), and positional analysis with FDR ≤0.05 were considered significant, and the top 50 enriched gene ontology (GO) terms with FDR ≤0.05 for GO-biological process (BP) and GO-cellular component (CC) analysis were filtered. Transcription factor analysis was conducted using the MetaCore Transcription Regulation algorithm with the default settings (MetaCore™ version 22.1, build 70800, https://portal.genego.com/) by uploading the ENSEMBL IDs of the DEGs with their fold-changes and q-values. The UCSC human genome browser was used to map the genes enriched on specific cytogenic bands (https://genome.ucsc.edu).

RNA isolation and reverse transcription-quantitative (RT-q) PCR. Total RNA was extracted using a RNeasy Mini Kit according to the manufacturer's instructions (Qiagen GmbH, cat. no. 74106). RNA quality and concentration were measured using a Nanodrop RNA 6000 nano-assay (for RT-qPCR). A total of 2 μg total RNA was reverse transcribed using a High-Capacity RNA-to-cDNA kit according to the manufacturer's instructions (Thermo Fisher Scientific, Inc; cat. no. 4387406) The cDNA sample was diluted by adding 60 μl nuclease-free water to make an estimated final concentration of 25 ng/μl. Then, 10 μl reaction mix was prepared by adding 1 μl cDNA, 0.5 μl target probe (FAM conjugated), 0.5 μl ACTB (VIC), 3 μl nuclease-free water, and 5 μl TaqMan Fast Advanced Master Mix (Thermo Fisher Scientific, Inc., cat. no. 4444557) and reactions were performed in accordance with the TaqMan Fast Reaction Protocol on an AB StepOnePlus Real-Time PCR System (Applied Biosystems; Thermo Fisher Scientific, Inc.). Data were analyzed using the DDCq method (25) and β-actin was used as the reference gene. The TaqMan probes for Real-time PCR were as follows: ACTB (Hs01060665_g1), USP14 (Hs00193036_m1), VAPA (Hs00427749_m1), NDUFV2 (Hs00221478_m1), TYMS (Hs00426586_m1), METTL4 (Hs01559838_m1), SEH1L (Hs01031566_m1), IMPA2 (Hs00274110_m1), MYL12B (Hs01050560_m1), S100A4 (Hs00243202_m1), TMSB4X (Hs03407480_gH), and FHOD1 (Hs01077922_m1).

Anchorage-independent growth

Metabolite rescue. A bottom layer of 0.6% noble agar in complete medium was prepared in 6 cm dishes. In metabolite rescue experiments, $1x10^3$ Control and shPSAT1 PC9 cells/dish were plated in 0.3% agar in RPMI-complete media supplemented with or without the indicated metabolite/s: No supplement (-); single metabolite, NEAA, Nucleoside, or 500 μM α-KG; double metabolites, (NEAA + 500 μM α-KG), (NEAA + Nucleoside), (Nucleoside + 500 μM α-KG); and all metabolites (NEAA+ Nucleoside+ 500 μM α-KG). Colonies were fed with 0.25% agar in RPMI complete medium with or without metabolite/s every 3-4 days during the 21-day incubation. At the end of the study, whole plate images were captured, and colonies were counted using ImageJ version 1.53 (National Institutes of Health). Dimethyl 2-oxoglutarate was used as the α-KG supplement.

Rescue with PSAT1 or nuclear acetyl-mimetic PKM2 expression. A bottom layer of 0.6% noble agar in a complete medium was prepared in 6 cm dishes. A total of $1x10^3$ PC9 cells/dish (Control-EV, shPSAT1-EV, and shPSAT1-FLAG-PSAT1 or shPSAT1-$PKM2^{NLS\text{-}K433Q}$) were plated in a 0.3% agar in RPMI complete media solution. Colonies were fed with 0.25% agar in RPMI complete medium every 3-4 days during the 21-day incubation. At the end of the study, whole plate images were captured, and colonies were counted using ImageJ.

Whole-cell protein extracts and subcellular fractionation. Total protein was extracted using Pierce IP lysis buffer supplemented with protease and phosphatase inhibitor cocktail according to the manufacturer's protocol (Thermo Fisher Scientific, Inc.; cat. no. 87787). Cytosolic and nuclear proteins were isolated using the NE-PER kit (Thermo Fisher Scientific, Inc. cat. no. 78835). A total of 15 μg cytoplasmic protein and 25 μg nuclear protein was used for immunoblotting analyses.

Immunoblotting. Proteins within the whole-cell lysates, cytosolic fraction, and nuclear fraction were resolved by SDS-PAGE and transferred to PVDF membranes. Membranes were blocked and then incubated with the indicated primary antibodies [PSAT1 1:1,000, β-catenin 1:1,000, PKM2 1:1,000, β-actin 1:5,000] overnight at 4°. Protein detection was performed using the appropriate HRP-conjugated secondary anti-mouse or anti-rabbit antibody (1:10,000) and visualized using a chemiluminescence reagent (ECL Prime, MilliporeSigma).

Luciferase reporter assay. Control-EV, shPSAT1-EV, and shPSAT1-FLAG-PSAT1 PC9 cells were plated into 6-well plates and transfected with 2 μg pGL4.49[luc2P/TCF-LEF/Hygro] using jetPEI with overnight incubation (media changed after 24 h). A total of 48 h post-transfection, stably transfected cells were selected using 200 μg/ml hygromycin (TCF-LEF vector), 200 μg/ml geneticin (pcDNA3.1 vector), and 1 μg/ml puromycin (shRNA vector). For each study, $4x10^5$ stable cells were plated into each well of a 6-well plate (3 replicates/condition). The following day, the media was replaced with serum-free media and maintained for 24 h. Cells were then harvested according to the Dual-Luciferase Reporter Assay protocol. Firefly luciferase activity was determined using a 96-well plate luminometer. Protein concentration was measured using a BCA Protein assay and used to normalize the luciferase activity.

Phalloidin staining. Cells were plated into 4-well chamber slides (Lab-Tek II Chamber slides, cat. no. 154526) and incubated in serum-free media for 24 h. Samples were then fixed with 3.7% paraformaldehyde in PBS solution for 10 min at room temperature and washed three times with PBS. Then, the cells were permeabilized with 0.1% Triton X-100 in PBS for 3 min and washed again. For visualization, cells were incubated with a Rhodamine Phalloidin (Invitrogen; Thermo Fisher Scientific, Inc., cat. no. R415) working solution (5 μl stock/200 μl PBS) for 20 min in the dark at room temperature. After three additional washes with PBS, slides were covered with SlowFade Diamond Antifade Mount with DAPI (cat. no. S36964) reagent. Images were captured using an Olympus FV-3000 confocal microscope equipped with Fluoview software (Olympus Corporation) at x40 magnifications.

Public microarray datasets analysis

Data search and import. The EGFR mutant lung cancer datasets were chosen based on the number of EGFR mutant tumor samples (n>10) with paired or unpaired normal tissue samples and the availability of relevant clinical information. According to these selection criteria, GSE31210, GSE27262, GSE31547, GSE31548, GSE32863, and GSE75037 datasets were imported to BRB-ArrayTool [version 4.6.1-Stable (June 2020)] using the NCBI GEO Series tool (26).

Identification of common gene sets. shPSAT1-mediated down-regulated and up-regulated gene lists obtained from the RNA-seq analysis were prepared separately as txt files and saved under the user gene list folder within the program files of ArrayTool. Expression of these genes was filtered using the ArrayTool-re-filter option and normalized. Genes whose expression was <20% of the expression data and <1.5-fold change in either direction from the gene's median value were excluded. DEGs from the RNA-seq profiling were directly compared to those gene changes between EGFR mutant tumor and normal lung samples using the ArrayTool-Class Comparison plugin and the significance threshold of univariate analysis with P≤0.05 served as the statistical threshold for significance. This was done to identify which PSAT1-regulated genes from the RNA-seq screen were also differentially expressed in EGFR mutant NSCLC. Importantly, up-regulated genes in EGFR tumors should be down-regulated by shPSAT1 and vice-versa. Genes with fold-changes (EGFR mutant tumor/normal lung) ≥1.4 from the shPSAT1-down-regulated genes list and genes with fold-changes (EGFR mutant tumor/normal lung) ≤0.71 from the shPSAT1-up-regulated genes list were considered PSAT1-associated genes linked with EGFR mutant lung cancer. This procedure was repeated for each dataset (GSE31210, GSE27262, GSE31547, GSE31548, GSE32863, and GSE75037). Then, the common gene sets were determined using a Venn diagram (http://bioinformatics.psb.ugent.be/webtools/Venn/). The fold-change of common genes with the P-values and FDR-values from each dataset were extracted using the ArrayTool-Class Comparison tool.

Survival risk prediction with the common gene sets. Among the datasets, GSE31210 was the only set encompassing all the following clinical information on defined NSCLC genotypes: KRAS mutant and EGFR/KRAS wild-type tumor data in addition to EGFR mutant lung tumors and their pathological stage, relapse-free survival (RFS) and overall survival (OS) data [clinicopathologic characteristics of patient cohort described in (27)]. Survival predictions for OS and RFS using the expression data of the PSAT1-associated common gene lists were performed using the BRB-ArrayTool survival risk prediction function (28). Principal component analysis with leave-one-out cross-validation with 100 permutation tests was used to calculate prognostic indices and classified the patients as high-risk and low-risk groups. This analysis was then used to generate the permutated Kaplan-Meier survival plots, time-dependent receiver-operating characteristics (ROC) curves with area under the curve (AUC) values, and a table containing the predicted genes associated with survival with their cross-validated (CV) support % and covariant (wi) used in this study.

Identification of a potential PSAT1-associated metastatic gene signature. GSE14107 was imported as described above due to the presence of a genome-wide expression profile of both parental PC9 cells and its metastatic brain subline of PC9-BrM3 (29). The ArrayTool-Class comparison plugin determined DEGs with a significance threshold of univariate analysis of P≤0.05. Down-regulated and up-regulated gene lists were assigned based on fold-change (PC9-BrM3/PC9-Parental) ≥0.71 and ≤1.4, respectively. The GSE14107 gene list was compared with the differential expression gene list from the PC9-shPSAT1 RNA sequencing analysis using Venn diagrams to find common genes. A heatmap was generated using Cluster 3 (23) and Java Treeview (24).

Statistical analysis. Comparisons were performed based on the number of groups with one or more independent variables. A repeated-measures one-way ANOVA with a post-hoc Tukey's multiple comparisons test was used for comparisons between three groups (PSAT1 and nuclear PKM2 rescue studies). This data is presented in their respective figures as the mean ± SEM. For analysis of the soft agar assay with metabolite supplementation, a two-step analytical approach was used: First, a two-way ANOVA with a post hoc Dunnett's multiple comparison test was performed with raw data to examine the effect of metabolite supplementation on both control and shPSAT1 cells. Then, the ratio of colony numbers (shPSAT1/Control) within each treatment was used for the repeated measures one-way ANOVA with a post hoc Dunnett's multiple comparisons test to assess the effect of rescue. This data is presented as a box & whisker blot with error bars represented as 5-95%. All protein rescue and metabolite supplementation studies were statistically analyzed using Prism version 9 (GraphPad Software, Inc.). The number of experimental replicates for each analysis is stated within the figure legends. P≤0.05 was considered to indicate a statistically significant difference. All statistical analysis of the publicly available microarray data was performed with BRB-Array Tool. The class comparison tool was used to perform two-sample T-test for GSE27262, GSE31547, GSE31548, GSE32863, GSE75037, and GSE14107 and F-test with pairwise analysis (EGFR mutant Stage I/Normal and EGFR mutant Stage II/Normal) for GSE31210 for each gene. P≤0.05 served as the statistical threshold for significance. Statistical analysis for the survival predictions for OS and RFS using the expression data of the PSAT1-associated common gene lists was performed using the BRB-ArrayTool survival risk prediction tool function (28). Risk groups were generated through the supervised principal component method described in (30). The leave-one-out cross-validation (LOOCV) method was chosen to determine the survival risk groups and used to generate the cross-validated Kaplan-Meier survival curve and the estimation of cross-validated time-dependent receiver-operating characteristic (ROC) curves. Values with P<0.05 based on 100 permutations of the cross-validated log-rank statistics for the Kaplan-Meier survival curves and the area under the cross-validated ROC curves (AUC) were reported as statistically significant.

Results

Determination of DEG in PSAT1 silenced PC9 cells. Several reports have shown that metabolic enzymes translocate into

different cellular compartments, particularly the nucleus, to exert non-canonical functions (17,31,32). In our previous study, it was demonstrated that PSAT1 undergoes nuclear translocation in an EGFR activation-dependent manner in NSCLC cells (11). As a global transcript analysis with respect to PSAT1 depletion had yet to be reported in EGFR mutant NSCLC, a genome-wide gene expression profiling was performed using RNA-seq technology to uncover potential novel cellular processes altered by PSAT1 loss. A total of 279 down-regulated and 211 up-regulated genes were identified following PSAT1 silencing (Fig. 1 and Tables SI and II).

Pathways and biological processes affected by PSAT1 suppression. These PSAT1-related DEGs were interrogated using MSigDB (33). Both down-regulated and up-regulated genes were assessed separately by MSigDB and the top 20 KEGG pathways were plotted as $\log_{10}$(FDR) in the indicated pathways (Fig. 2A and B). This analysis identified genes associated with folate biosynthesis, glutathione metabolism, and purine and pyrimidine metabolism pathways impacted by PSAT1 silencing (Fig. 2A), suggesting that decreased SSP activity transcriptionally influences the serine biosynthetic pathway. In addition, down-regulated genes were enriched in well-known oncogenic pathways, including MAPK, P53, and TGFβ signaling pathways, base excision repair, and the cell cycle (Fig. 2A). Paradoxically, KEGG pathway analysis of up-regulated genes also found cancer-related pathways involving the MAPK signaling pathway, ERBB signaling pathway, pathways in cancer, and endometrial cancer (Fig. 2B). As the DEGs enriched in KEGG pathway analysis represented a small portion of DEGs (25/211 up, 58/279 down), further exploration was required to obtain a broader understanding of processes impacted by PSAT1 loss.

GO analysis was performed using the MSigDB- GO-BP (Biological Process) and GO-CC (Cellular Component) tools with the top 50 signatures (FDR ≤0.05; Figs. 2C, D, S1A and B). In line with the KEGG pathways, down-regulated genes were enriched in the GO-BP headings of cell cycle, cell proliferation, nucleotide-related metabolism, and migration (Fig. 2C), while the protein products of these genes primarily function within the nucleus or are associated with the cytoskeleton (Fig. S1A). Interestingly, GO-BP processes related to immune response, such as locomotion, immune system processes, and defense response, were enriched in GO analysis of up-regulated genes (Fig. 2D) and found to function within Golgi-ER trafficking and secretion-related pathways (Fig. S1B). These observations implicate the involvement of PSAT1 in various cellular processes and highlight a requirement for functional studies to elucidate the contribution of PSAT1 to these pathways.

PSAT1 contributes to anchorage-independent growth, in part, by providing metabolites for serine-glycine-one carbon metabolism. The KEGG analysis of shPSAT1-mediated down-regulated genes identified metabolic pathways necessary for cell division, such as purine/pyrimidine metabolism and folate biosynthesis (Fig. 2A). Similarly, GO analysis of down-regulated genes were implicated in DNA metabolism and cell proliferation (Fig. 2C). As a result, loss of PSAT1 appears to impact key metabolic macromolecules that contribute to the oncogenic capacity of EGFR mutant NSCLC cells

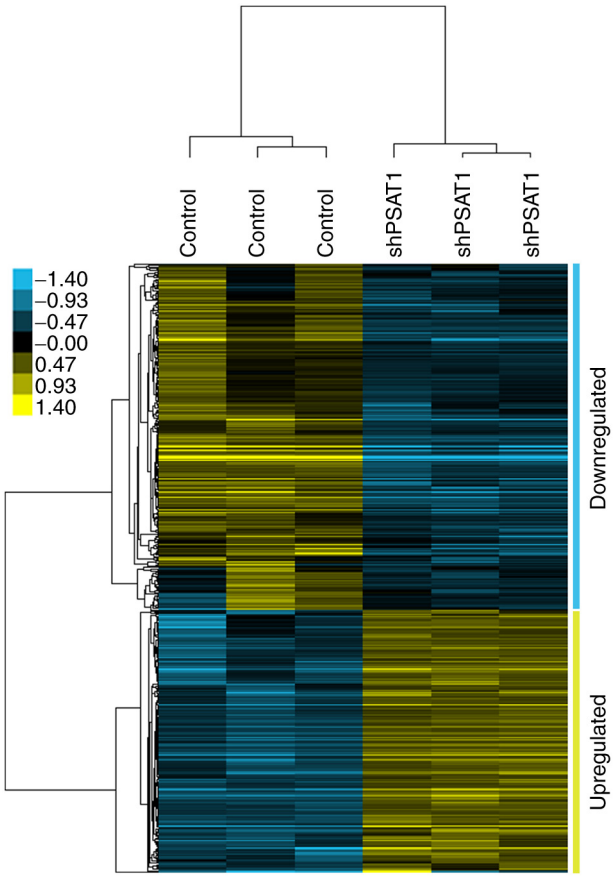

Figure 1. Heatmap showing the differentially expressed genes following PSAT1 silencing in PC9 cells. Genes with an FPKM value (Control or shPSAT1) ≥5 and q-value ≤0.05 were filtered and included in the analysis. A Log_2(shPSAT1/Control) value ≤-0.48 was considered to be downregulated and a Log_2(shPSAT1/Control) value ≥0.48 was considered to be upregulated. Downregulated and upregulated genes are listed in Tables SI and II, respectively. sh, short hairpin; PSAT1, phosphoserine aminotransferase 1; FPKM, Fragments per kilobase of transcript per million mapped reads.

(Fig. 3A). To interrogate this, soft agar assays were performed in the absence of PSAT1 with or without supplementation of SSP-downstream metabolites, including NEAA, nucleosides, and α-KG. Initially, it was observed that depletion of PSAT1 resulted in a 40% reduction in colony formation compared to control cells (Fig. 3B) and that this defect was specific to PSAT1 depletion since the restoration of PSAT1 expression was able to fully rescue anchorage-independent growth (Fig. 3C). Yet, the addition of individual downstream metabolites alone did not affect the loss of colony formation upon PSAT1 suppression. However, combining any metabolite(s) with nucleosides significantly increased colony number in the absence of PSAT1 compared with media without supplementation (Fig. 3B). Together, these results are consistent with a metabolic requirement for PSAT1 for anchorage-independent growth.

Our previous study demonstrated that loss of PSAT1 inhibited the nuclear localization of PKM2 and that expression of a nuclear acetyl-mimetic form of PKM2 partially rescued cell motility in PSAT1-silenced cells (11). Thus, whether this nuclear acetyl-mimetic form of PKM2 ($\text{PKM2}^{\text{NLS-K433Q}}$) also contributed to PSAT1-driven anchorage-independent growth was assessed here. It was found that $\text{PKM2}^{\text{NLS-K433Q}}$ expression

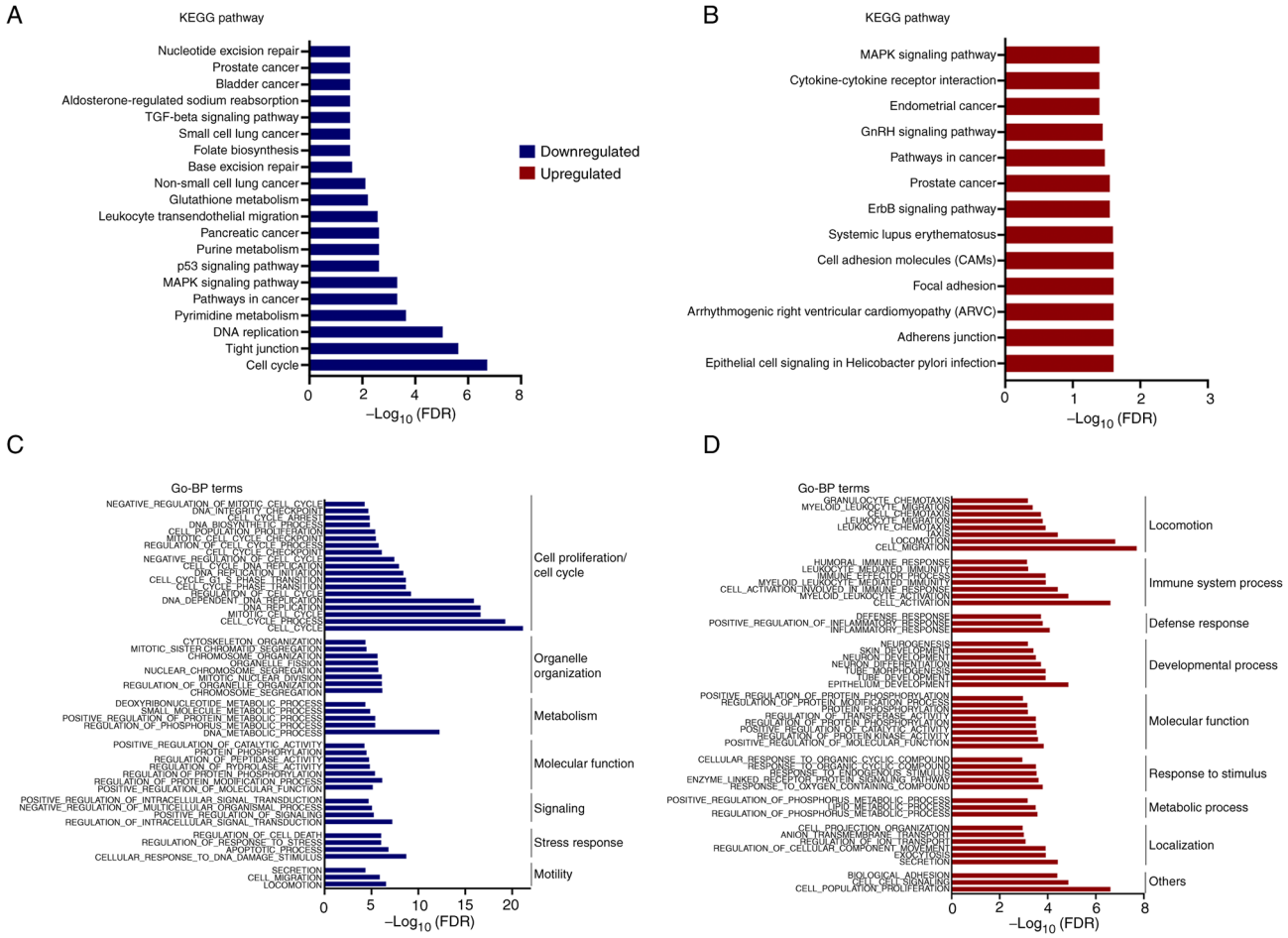

Figure 2. Functional analysis of differentially expressed genes. (A and B) KEGG pathway analysis showing the top 20 altered pathways following PSAT1 silencing in PC9 cells based on the (A) shPSAT1-downregulated and (B) shPSAT1-upregulated genes. (C and D) GO analysis showing the BPs impacted by PSAT1 silencing in PC9 cells based on the (C) shPSAT1-downregulated and (D) shPSAT1-upregulated genes. sh, short hairpin; PSAT1, phosphoserine aminotransferase 1; GO, Gene Ontology; KEGG, Kyoto Encyclopedia of Genes and Genomes; BP, biological processes.

failed to restore soft agar colony formation in the absence of PSAT1 (Fig. S2). These findings suggest that nuclear PKM2, while necessary for cell motility, is dispensable for PSAT1-mediated anchorage-independent growth.

PSAT1 loss modulates the expression of actin-binding proteins and rearranges the actin-cytoskeleton. In our previous study it was demonstrated that reduced cell migration upon PSAT1 silencing could be partially rescued by nuclear acetyl-mimetic PKM2 (11), the lack of complete rescue prompted exploration of other cell migratory processes that may be influenced by PSAT1. GO analysis found enrichment of shPSAT1-down-regulated genes that are involved in actin cytoskeletal organization (Figs. 2C and S1A). It is well-established that the actin cytoskeleton not only determines cellular morphology but plays key roles in migration and invasion due to the requirement for cell movement (34). To interrogate this, the PSAT1-mediated DEGs were assessed to identify genes involved in actin-related processes. Fig. 4A shows the DEGs related to actin binding or the actin cytoskeleton. To assess a PSAT1 functional requirement for cytoskeletal arrangement, phalloidin staining was performed to monitor filamentous actin (F-actin) formation in the presence or absence of PSAT1 expression. Immunofluorescence microscopy found that PC9 cells exhibited structured actin fibers spanning the whole cell body, while cells devoid of PSAT1 displayed loss of these actin stress fibers (Fig. 4B). Yet, re-expression of PSAT1 in silenced cells rescued long fiber formation, thereby validating the on-target effects of PSAT1 and confirming a role for PSAT1 in actin cytoskeletal organization.

Next, PSAT1-regulation of actin-related genes directly involved in F-actin formation was verified (Fig. 4C). Transcript analysis found that PSAT1 silencing reduced *FHOD1*, *TMSB4X*, and *S100A4* levels, which were rescued via PSAT1 re-expression (Fig. 4C). Coupled with the cytoskeletal analysis, these results validate our transcriptomic findings and implicate a new role for PSAT1 in cell migration through regulating the expression of actin-related factors and influencing cytoskeletal rearrangement.

Transcriptional analysis validates a link between PSAT1 and the RB/E2F pathway. To further understand the effect of PSAT1 on gene expression, MSigDB CGP analysis was performed based on the gene set analysis of the shPSAT1-DEGs (Fig. S3). Genes down-regulated upon PSAT1 loss were significantly enriched in the 'FISCHER_ G1_S_CELL _CYCLE' and 'CHICAS_RB1_TARGETS_SENESCENT' datasets (Fig. S4A) and MetaCore transcription factor network analysis

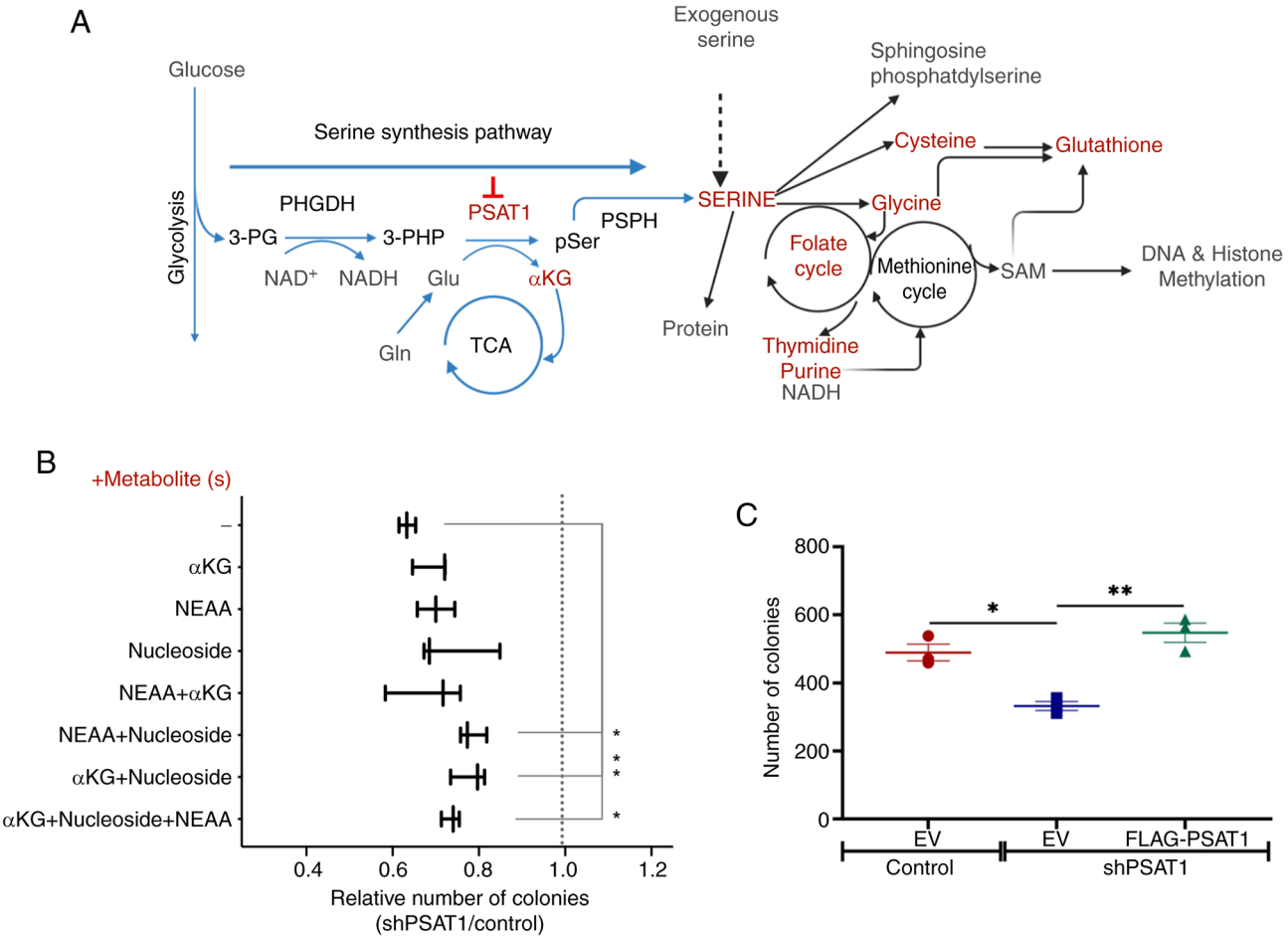

Figure 3. PSAT1 metabolic activity contributes to anchorage-independent growth. (A) Schematic representation of the serine biosynthesis pathway. Transcriptionally impacted metabolic pathways following PSAT1 silencing are highlighted in red. (B) Soft agar assay assessing the effect of the addition of downstream metabolite/s on colony formation in the PSAT1 silenced PC9 cells. The mean number of colonies in the control group for each condition was set to 1 (dashed line) and the ratio of colony numbers (shPSAT1/Control) is shown as a boxplot (n=3). Metabolites added included 500 μM α-KG, 1x NEAA, or 1x nucleosides. (C) Analysis of soft agar assay confirming specificity for PSAT1 on PC9 colony formation (n=3). shPSAT1-EV and shPSAT1-FLAG-PSAT1 cells represent PSAT1 silenced and re-expressed cells, respectively. *P≤0.05, **P≤0.01. EV, empty vector; sh, short hairpin; PSAT1, phosphoserine aminotransferase 1; α-KG, α-ketoglutarate; NEAA, Non-essential amino acids including serine and glycine.

found E2F1 as a major regulator of these DEGs (Table SIII and Fig. S4B). Despite the presence of certain up-regulated genes, most genes within the E2F1 transcriptional network, including E2F1, were decreased upon PSAT1 suppression (Fig. S4B). Taken together, the *in-silico* analysis indicated that PSAT1 regulated E2F1 transcriptional activity.

PSAT1 levels impact β-catenin expression and transactivation. EGFR activation promotes the nuclear localization of β-catenin through various mechanisms (35). While phosphorylation of membranous β-catenin by EGFR or AKT leads to migration of β-catenin away from the membrane, EGFR activation inhibits the proteasomal degradation of cytoplasmic β-catenin protein by GSK3β inactivation. Thus, both EGFR-mediated pathways result in the accumulation of β-catenin in the nucleus and seem to contribute to every step within EGFR-driven tumor progression (36-39). While previous studies have linked PSAT1 to inhibition of GSK3β in multiple tumor types (7,14,15), the association between β-catenin and PSAT1 remains elusive in EGFR mutant NSCLC cells. Furthermore, nuclear PKM2 requires EGF-induced β-catenin transactivation in EGFR-driven tumor growth of GBM and EGF-induced epithelial-to-mesenchymal transition and invasion in HCC cells (31,40). Considering these prior reports and our results showing the link between PSAT1 and nuclear PKM2 (11), it was speculated that loss of PSAT1 may result in altered β-catenin transactivation.

Interrogation of the CGP analysis found differential expression of genes within the 'FEVR_CTNNB1_TARGETS_DN' and 'WANG_RESPONSE_TO_GSK3B_INHBITOR_SB216763_DN' gene sets, which indicated a possible regulatory role for PSAT1 on β-catenin function (Fig. S5A). β-catenin induces transcription via interacting with TCF (T-cell specific transcription factor)/LEF1 transcription factor family (41,42). Notably, TCF7L1 (TCF3) and TCF7L2 (TCF4) were found to be changed by PSAT1 loss in the MetaCore transcription analysis (Table SIII). As TCF7L1 is a known repressor (42) and is up-regulated by PSAT1 silencing (Fig. S5B, red circle), it was hypothesized that there would be reduced β-catenin transactivation. However, up- and down-regulated genes were identified within the TCF3 and TCF4 networks (Fig. S5B and C). In short, while supportive, these analyses

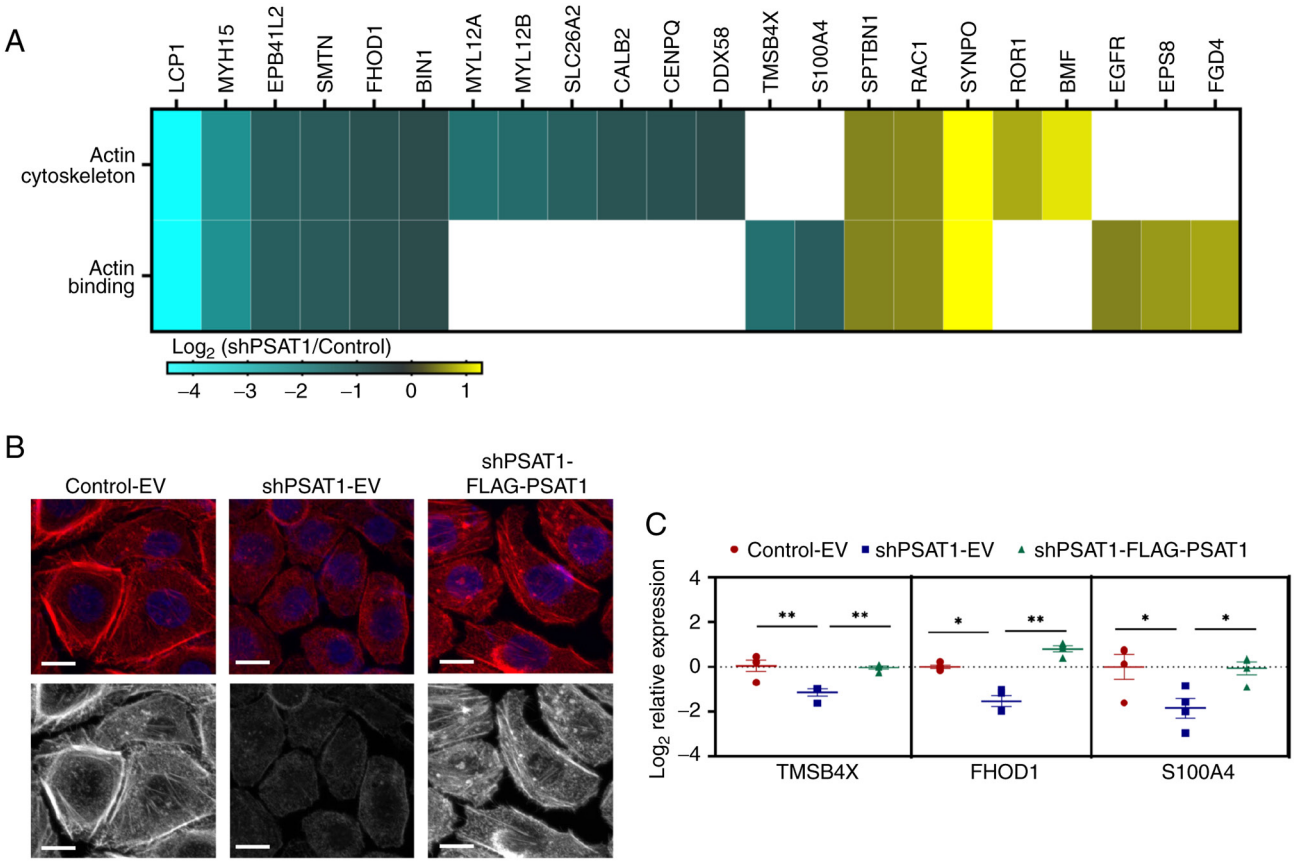

Figure 4. PSAT1 is involved in actin-cytoskeleton rearrangement and regulates the expression of actin-related proteins. (A) Heatmap demonstrating differentially regulated actin-related genes following PSAT1 silencing. (B) Immunofluorescence analysis showing PSAT1 relevance on F-actin formation in PC9 cells. Phalloidin [red and gray (pseudo-colored)] was used to stain F-actin. DAPI (blue) was used to stain the nucleus (n=3). Scale bar, 10 μm. (C) Reverse transcription quantitative-PCR was used to validate the regulation of genes involved in F-actin formation by PSAT1 (n=3-4). shPSAT1-EV and shPSAT1-FLAG-PSAT1 cells represent the PSAT1-silenced and re-expressed cells, respectively. *P≤0.01, **P≤0.001. EV, empty vector; sh, short hairpin; PSAT1, phosphoserine aminotransferase 1.

were unable to provide clear insights into whether β-catenin transactivation may change upon PSAT1 silencing.

To better understand the association between PSAT1 and β-catenin, whether β-catenin protein expression was altered in the absence of PSAT1 was next assessed. Immunoblot analysis found that β-catenin expression decreased upon PSAT1 silencing, which can be rescued by re-expression of PSAT1 (Fig. 5A). Yet, nuclear PKM2 expression (PKM2$^{NLS-K433Q}$) had no effect on β-catenin expression under PSAT1 silencing, indicating that regulation of β-catenin expression is independent of nuclear PKM2 in the context of PSAT1 loss (Fig. S6).

Accumulation of cytoplasmic β-catenin due to inhibited proteasomal degradation leads to its nuclear localization and transactivation (43,44). Since a reduction in total β-catenin levels was observed here, its cellular distribution upon PSAT1 silencing was examined. Subcellular fractionation found that nuclear β-catenin expression decreased in PSAT1 silenced cells in comparison with control cells, which could be rescued upon re-expression of PSAT1 (Fig. 5B).

The same pattern of β-catenin expression was also observed in the cytoplasmic fraction. According to the RNA-Seq analysis, loss of PSAT1 did not alter the mRNA expression of β-catenin (data not shown), which implies that PSAT1 potentially contributes to β-catenin stability in PC9 cells, possibly through increasing phospho-GSK3β levels.

Next, the β-catenin transcriptional activity was measured directly using a luciferase reporter assay (luc2p/TCF-LEF). Loss of PSAT1 in serum-starved cells led to significantly reduced β-catenin activity, which was rescued upon PSAT1 restoration (Fig. 5C). Taken together, these results suggest that PSAT1 increases β-catenin expression and transactivation, most likely through regulating protein stability.

Identification of differentially expressed PSAT1-associated genes in primary EGFR mutant NSCLC. PC9 cells have frequently been used as an *in vitro* model for EGFR mutant lung cancer due to the presence of an activation mutation (exon19del) in the EGFR tyrosine kinase domain and their responsiveness to EGFR tyrosine kinase inhibitor treatment (45). Within the above transcriptomic analysis, RNA was collected from serum-starved PC9 cells to assess the EGFR-dependent gene expression alterations while minimizing the contribution of other serum factors from the media. Therefore, it was hypothesized that a subset of PSAT1-mediated genes would be observed that have been independently implicated in EGFR-driven lung tumorigenesis. To identify these genes, a bioinformatics approach was used through comparative analysis between the differentially regulated genes in our RNA-seq analysis and publicly available microarray datasets obtained from EGFR mutant patient tumors (Fig. S7).

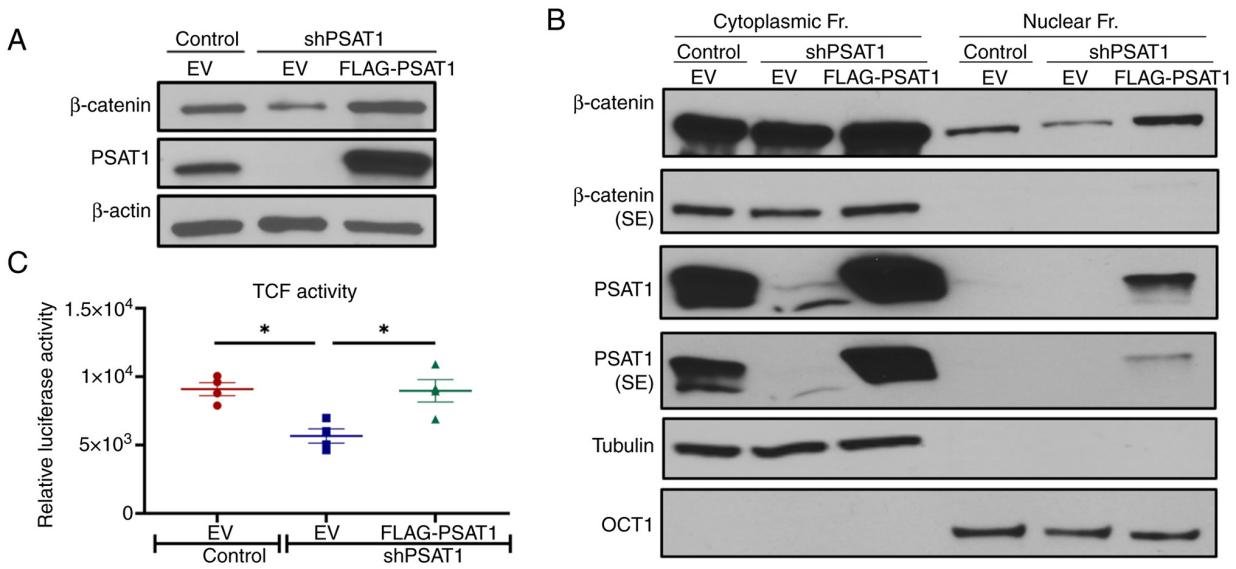

Figure 5. Loss of PSAT1 impacts β-catenin expression and transcriptional activity. (A and B) Representative immunoblot showing regulation of β-catenin expression by PSAT1 in (A) the whole cell lysate (n=3), and (B) in the cytoplasmic and nuclear fractions (n=3). (C) TCF-luciferase activity showing the reduction in β-catenin/TCF transcriptional activity following PSAT1 silencing, which was rescued by PSAT1 re-expression (n=4). shPSAT1-EV and shPSAT1-FLAG-PSAT1 cells represent the PSAT1-silenced and re-expressed cells, respectively. *P≤0.05. SE, short exposure; EV, Empty vector; sh, short hairpin; PSAT1, phosphoserine aminotransferase 1; TCF, T-cell specific transcription factor; OCT1, POU class 2 homeobox 1.

The GEO database was searched for datasets containing transcriptional analysis of EGFR mutant lung tumors and normal lung tissues (n≥10, each) derived from untreated patients. Based on these criteria, GSE31210, GSE31547, GSE31548, GSE27262, GSE32863, and GSE75037 datasets were chosen for subsequent analysis. Gene lists derived from the GSE31547 and GSE31548 datasets were combined as 'GSE31547-48' since expression profiles were obtained from the same patients but neither Affymetrix-HG-U133A nor Affymetrix-HG-U133B can cover all genes from our RNA-seq list (Table SIV) (46). Class comparison analysis was then conducted using the BRB-ArrayTool to determine the DEGs from our PSAT1-DEG list (26). PSAT1-associated genes were defined as those up-regulated in tumor tissues compared to normal lung that are correspondingly down-regulated upon PSAT1 silencing in our RNA-seq profiling (shPSAT1-down-regulated) and, conversely, down-regulated in tumor tissue that are correspondingly up-regulated upon PSAT1 loss (shPSAT1-up-regulated).

The PSAT1-associated gene list from each dataset was then compared to obtain 'common genes' altered across all datasets. A total of 13 genes from the shPSAT1-down-regulated gene list and 12 genes from the shPSAT1-up-regulated gene list that were differentially expressed in EGFR mutant tumors compared to normal lung tissue were identified (Fig. 6A and B, respectively). Together, these were designated as a PSAT1-associated gene signature in EGFR mutant lung tumors (Table SV and SVI). This bioinformatics approach was able to identify common genes linked through PSAT1 regulation in EGFR mutant lung tumors.

A PSAT1-associated gene expression signature correlates with poorer outcomes in patients with EGFR mutant lung cancer. Next, the prognostic value of this PSAT1-associated gene signature in EGFR mutant lung cancer was assessed. Among the five publicly available datasets, the GSE31210 was used as it included all relevant clinical information such as NSCLC genotype (127 EGFR mutant tumors), staging (EGFR mutant tumors: IA: n=77, IIB: n=26, II: n=24), and patient outcomes (RFS and OS) (Table SIV), whereas the other datasets had a limited number of EGFR mutant lung cancer samples for survival analysis and could not be combined due to platform incompatibility.

The BRB-ArrayTool survival risk prediction tool was utilized to perform OS and RFS analysis as previously described (28). To validate this 25-gene signature in patient samples, principal component analysis with leave-one-out cross-validation and log-rank statistics with 100 permutation tests was used to calculate the prognostic indices and classify the patients as high-risk and low-risk groups. According to the KM analysis for OS, the high-risk group (defined by 13 genes out of 25; Table SVII) exhibited a significantly shorter OS than the low-risk group with a prediction accuracy AUC value of 0.77 (Figs. 7A and S8A). Survival risk prediction analysis found additional genes (17 genes out of 25; Table SVII) that contributed to RFS. The KM plot demonstrated that the high-risk group correlated with a worse RFS with a prediction accuracy AUC value of 0.72 (Figs. 7D and S8D). Corresponding genes involved in RFS and OS prediction are summarized in Table SVII and VIII, which detail their corresponding relevant statistics used in survival risk score calculation and known roles in lung tumorigenesis, respectively. Probes/genes with positive coefficients (wi) in Table SVII indicate that higher expression correlates with shorter survival, whereas negative coefficients imply that higher expression is associated with longer survival. Down-regulated genes upon PSAT1 silencing possessed positive coefficients and up-regulated genes had negative coefficients, corroborating the findings above that the PSAT1-associated gene signature in EGFR mutant lung cancer is associated with worse outcomes.

A (i)

GSE ID #	# Probes	# Genes
27262	81	61
31210	147	102
31547-48	43	34
32863	39	34
75037	75	59
Overall number of genes		**129**

(ii)

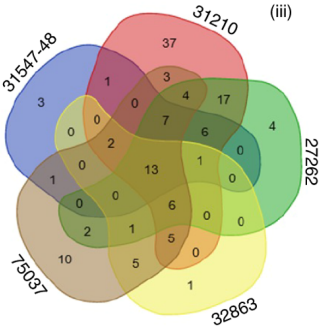

(iii)

Downregulated genes
PSAT1
TYMS
CDCA7
SFN
SLC39A4
UHRF1
MMP15
NSUN5
NETO2
PAICS
ANKRD22
SPAG4
MCM2

B (i)

GSE ID#	# Probes	# Genes
27262	90	51
31210	121	56
31547-48	54	36
32863	36	32
75037	61	50
Overall number of genes		**87**

(ii)

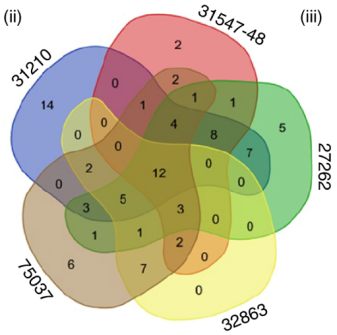

(iii)

Upregulated genes
HBEGF
BTG2
JAG1
TJP2
CFD
GPRC5A
SPTBN1
SCEL
EFNB2
S100A9
ALOX5
FILIP1L

Figure 6. Identification of a PSAT1-associated gene signature in EGFR mutant NSCLC. (A) shPSAT1-downregulated and (B) shPSAT1-upregulated genes that are differentially expressed in EGFR mutant NSCLC tumors compared with normal lung tissue were used to (i) plot tables summarizing the number of PSAT1-regulated differentially expressed genes within EGFR mutant tumor datasets, (ii) plot Venn diagrams demonstrating the number of common genes between datasets and (iii) create lists of common genes among all data sets. sh, short hairpin; PSAT1, phosphoserine aminotransferase 1; NSCLC, non-small cell lung cancer; EGFR, epidermal growth factor receptor; GSE, Gene Expression Omnibus.

In addition to EGFR mutant lung tumors, the GSE31210 microarray dataset also harbors ALK-fusion positive, KRAS mutant, and EGFR/KRAS/ALK wild-type tumor samples with their corresponding clinical information. Therefore, whether the predictive ability of PSAT1-associated gene signature applied to NSCLC tumors with other oncogenic drivers was assessed. Survival analysis for ALK-fusion positive tumors was excluded due to the limited sample size (n=10) and EGFR/KRAS/ALK wild-type tumors were defined as EGFR/KRAS wild-type. Survival risk prediction analysis for KRAS mutant (n=20) and EGFR/KRAS wild-type (n=68) tumors was then conducted as described above. Genes within the defined PSAT1-associated signature were unable to significantly separate high-risk and low-risk groups for both OS and RFS in either the KRAS mutant (Figs. 7B, E, 8B and E) or EGFR/KRAS wild-type tumors (Figs. 7C, F, S8C and F).

RFS-related genes can distinguish the high-risk group in patients with EGFR mutant Stage I NSCLC. The expression of the 17 PSAT1-signature RFS genes (Table SVII) from EGFR mutant tumors and normal lung tissue in the GSE31210 dataset were used for cluster analysis. As illustrated in Fig. 8, the high-risk group identified by RFS analysis clustered together and exhibited an opposite expression profile compared to that from the normal lung tissue. More notably, this analysis could selectively distinguish between high and low-risk groups even among clinical stage I patient samples (Stage 1, n=103; Stage 2, n=24). This implies that this PSAT1-associated gene signature may be predictive for high-risk groups within patients with stage I EGFR mutant NSCLC.

Discussion

PSAT1 expression is increased in several types of cancer, including NSCLC, and is associated with poor patient outcomes (15,47,48). While its metabolic function within SSP activity contributes to cell proliferation and tumor growth, oncogenic signals may result in the gain of alternative functions that promote tumor progression; particularly as nuclear localization of PSAT1 in EGFR-activated lung cancer cells was observed in our previous study (11). To gain a better insight into the role of PSAT1 in tumorigenesis, genome-wide expression profiling by RNA-seq technology was performed. DEGs were interrogated using bioinformatics-based tools for comparison with other gene expression datasets.

Inhibition of serine biosynthetic pathways blocks the production of precursors for folate, glutathione, and nucleotide biosynthesis, resulting in tumor growth arrest (5,6,49,50). The present study found down-regulation of genes within these pathways following PSAT1 silencing, adding another layer of regulation of these pathways by SSP. Impaired anchorage-independent growth by PSAT1 silencing was partially restored by downstream metabolite supplementation, supporting the metabolic function of PSAT1 within the serine biosynthetic pathway. PSAT1 is also implicated in inhibiting GSK3β-dependent phosphorylation and proteasomal degradation of target proteins (14,15,51). PSAT1-mediated stabilization of cyclin D1 promotes E2F transactivation in NSCLC cells, resulting in cell cycle progression and proliferation (15). Furthermore, transcriptomic analysis from patients with NSCLC identified the enrichment of E2F target expression in PSAT1-high tumors compared with PSAT1-low tumors. The *in-silico* analysis further supported this by demonstrating a reduction of E2F target genes following PSAT1 silencing. β-catenin was another potential target for the PSAT1/GSK3β pathway and is implicated in EGFR mutant lung tumorigenesis (14,36,37). Both bioinformatics analysis and functional results in the present study corroborated these previous findings that PSAT1 may be involved in the regulation of β-catenin stability and activity. These observed gene expression changes upon PSAT1 silencing support the known tumorigenic functions of PSAT1.

Myocardin-related transcription factors/serum-response factor (MRTF/SRF) signaling is a well-established pathway that promotes cell motility via transcriptionally regulating the expression of actin cytoskeleton-related genes (52,53). As MRTFs are actin-binding proteins, a higher

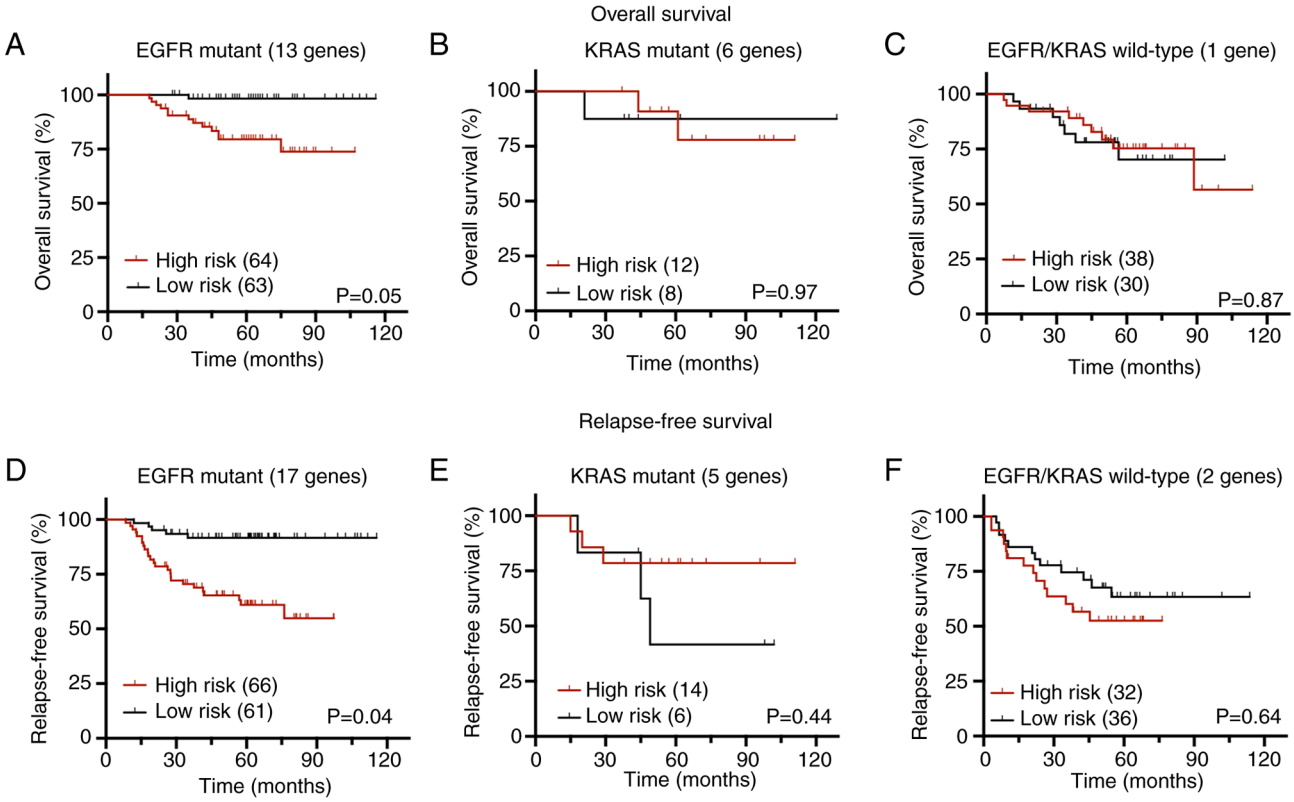

Figure 7. Prognostic potential of a PSAT1-associated gene signature in NSCLC with different genetic status. Cross-validated Kaplan-Meier curve and log-rank statistics based on permutation for overall survival in patients with (A) EGFR mutant, (B) KRAS mutant, and (C) EGFR/KRAS wild-type NSCLC and relapse-free survival in patients with (D) EGFR mutant, (E) KRAS mutant and (F) EGFR/KRAS wild-type NSCLC based on the GSE31210 dataset. PSAT1, phosphoserine aminotransferase 1; NSCLC, non-small cell lung cancer; EGFR, epidermal growth factor receptor.

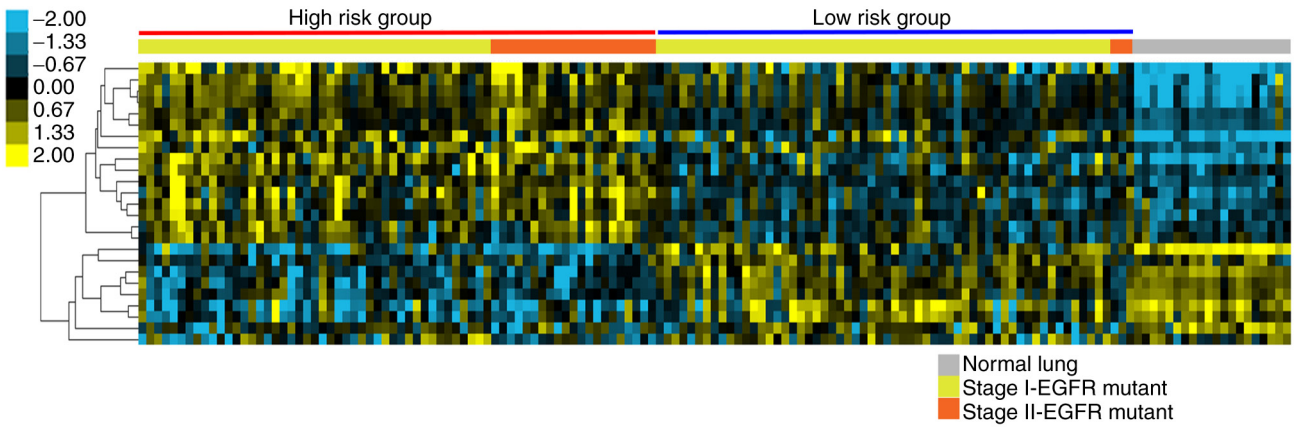

Figure 8. Heatmap showing the expression profile of the PSAT1-signature genes related to RFS in EGFR mutant NSCLC. The PSAT1 gene signature discriminates high-risk relapse stage 1 patients from low-risk stage 1 or 2 patients with EGFR mutant NSCLC (GSE31210). PSAT1, phosphoserine aminotransferase 1; NSCLC, non-small cell lung cancer; RFS, relapse-free survival; EGFR, epidermal growth factor receptor; GSE, Gene Expression Omnibus.

monomeric/polymeric actin ratio results in the sequestration of MRTFs in the cytoplasm, thereby reducing SRF-dependent gene expression. Formin Homology 2 Domain Containing 1 (FHOD1) functions as an actin filament capping and bundling protein and enhances cell migration by inducing the formation and stabilization of F-actin at the leading edge (54-58). Furthermore, the observation of elevated expression at the invasive front of squamous cell carcinoma further supports its role in cancer metastasis (57). Thymosin β4, encoded by TMSB4X, is another actin-binding protein that exhibits a G-actin sequestering function that inhibits spontaneous actin polymerization (59). It contributes to cell motility by localizing the monomeric G-actin at the leading edge of lamellipodia for actin polymerization, leading to membrane protrusions (60). Thymosin β4 has also been reported as a prognostic factor for poor survival and metastasis in patients with early-stage NSCLC (61). In addition, S100A4 is a well-recognized metastasis-associated protein that functions as a binding partner for actin-related factors such as actin, myosin, and tropomyosin (34,62). A recent report

showed that FHOD1-loss-driven MRTFA accumulation in the cytoplasm impacted cell motility in melanoma cells (63). Another study found that TGF-β-induced thymosin β4 expression enhanced MRTF/SRF transcriptional activity, potentially through sequestering monomeric actin binding to MRTFs (64,65). As the analysis found that PSAT1 silencing altered the expression of several actin cytoskeleton-related genes, including FHOD1 and TMSBX4 (thymosin β4), it will be intriguing to investigate the involvement of the MRTF/SRF pathway in PSAT1-mediated cytoskeleton rearrangement and cell migration.

Genes involved in immune response and leukocyte migration/chemotaxis were upregulated upon PSAT1 silencing (Fig. 2D). In addition, the protein products of these genes are localized in the Golgi, within the membrane and lumen of vesicles, and secretory membranes, suggesting a change in vesicle-mediated transport and secretion (Fig. S1B). As tumor-secreted factors contribute to immune cell infiltration into the tumor microenvironment, the results of the present study suggested that intratumoral PSAT1 may influence reprogramming within the tumor microenvironment (66,67). While immune checkpoint inhibitors (ICI) have been adopted as a therapeutic option for patients with NSCLC, patients with EGFR mutant lung cancer are excluded from this option since these patients have shown limited responses to ICI treatment (68). Thus, it is intriguing to investigate how tumoral PSAT1 may modulate the tumor microenvironment and whether targeting PSAT1 activity may sensitize EGFR mutant lung tumors to ICI treatment (69).

A literature search for the reported function of the identified survival genes in lung cancer was thus performed, and the findings are summarized in Table SVIII. It was observed that shPSAT1-down-regulated genes (which are conversely increased in tumors) were associated with a poor patient outcome and tumor progression and were involved in various oncogenic processes, including cell cycle progression, proliferation, migration, and invasion. Conversely, shPSAT1-up-regulated genes (which are conversely decreased in tumors) have been linked to a better prognosis and played roles in inhibiting cell proliferation, migration, and invasion. Among these genes, B-cell translocation gene 2 and G Protein-Coupled Receptor Class C Group 5 Member A (GPRC5A) have already been identified as tumor suppressors and GPRC5A acts as a negative regulator of EGFR signaling in NSCLC cells [3-5]. However, a relationship between these genes and EGFR mutant lung tumors in the current literature was not found, implying the novelty of the PSAT1-associated genes in EGFR mutant lung cancer.

The PSAT1-associated gene signature was primarily dominated by early-stage EGFR mutant lung cancer transcriptomic profiles due to the presence of a high number of stage I patients in GSE31210 (n=103) and GSE27262 (all stage I tumors). Due to the lack of advanced tumor samples, PSAT1-associated genes involved in late-stage tumor progression and metastasis may be lost. Through an examination of distinct datasets (GSE14107), which encompass transcriptomic profiles of the parental PC9 cell line (PC9-P) and a brain metastatic subline (PC9-BrM3) (29), a total of 81 common genes that were differently expressed following PSAT1 depletion and brain selective metastatic potential were found, which were considered as potential PSAT1-associated pro-metastatic genes (Fig. S9, Table SIX). Yet, the functional connection between PSAT1 and these putative pro-metastatic genes requires further investigation within an EGFR mutant NSCLC metastatic model.

Nuclear localized metabolic enzymes, including PDC, ACLY, and α-KGDH are involved in epigenetic regulation by providing a substrate for histone modifications (17,70,71). Accordingly, in our previous study, it was demonstrated that PSAT1 localizes to the nucleus in EGFR-activated NSCLC cells (11). Recent studies have found a link between PSAT1 and epigenetic alteration/remodeling/landscaping. Particularly, PSAT1 contributed to S-adenosylmethionine production for DNA retrotransposon methylation in Kras-mutant-Lkb1 loss pancreatic adenocarcinoma mouse models (72). Another study revealed that PSAT1 contributed to the maintenance of pluripotency of embryonic stem cells by supplying α-KG for enzymes that account for histone and DNA demethylation (73). Expression of adjacent genes can be regulated by epigenetics and is known as long-range epigenetic silencing or activation (74,75). Therefore, it is hypothesized that PSAT1 could epigenetically regulate the expression of genes located throughout the same chromosomal region. For this, positional gene set analysis was performed in MSigDB and found that 10% of the shPSAT1-down-regulated genes were enriched on the chr18p11 cytogenic band, while the chr7p21 cytogenic band harbored various shPSAT1-up-regulated genes (Fig. S10A). A previous report demonstrating the association of chr18p11 with non-smoker lung cancer susceptibility in a Korean population, which has a higher proportion of EGFR mutant NSCLC, prompted the examination of these genes localized in chr18p11 in response to differential PSAT1 expression in our previous study (76). The down-regulated genes identified were not restricted to a localized region but spanned a large area within chr18p11 (Fig. S10B). PSAT1-regulation of genes within this locus was confirmed using qPCR (Fig. S10C). The results suggested putative long-range gene expression regulation by PSAT1 within this genetic locus, yet further investigation is required to determine how PSAT1 may contribute to epigenetic regulation in this region.

In summary, these experiments examined genome-wide expression changes upon PSAT1 silencing using gene profiling and bioinformatics approaches. The analysis corroborated previous findings on the role of PSAT1 within the serine biosynthetic pathway in regulating E2F activity and β-catenin protein expression/transcription activity. In addition, rescue of F-actin stress fibers and expression of actin-related genes by restored PSAT1 validated a functional role for PSAT1 on cytoskeletal structure. A PSAT1-dependent gene signature that may have prognostic value regarding patient outcomes in EGFR mutant NSCLC was also identified. Together, these findings suggest that targeting PSAT1 may have clinical utility in this patient population. To date, no PSAT1 inhibitors have been described, but several PHGDH antagonists have been pre-clinically evaluated against multiple tumor types (6). This approach assumes that the changes observed upon PSAT1 silencing in this context are solely related to the metabolic activity of PSAT1 and that targeting other SSP enzymes would yield identical results. In our previous study, it was demonstrated that PSAT1 exhibits differential compartmentalization

under EGFR activation and is necessary for nuclear PKM2 translocation (11). Whether this activity is SSP-independent and/or significantly contributes to the overall pro-tumorigenic function of PSAT1 in EGFR mutant NSCLC is a focus of ongoing work and will ultimately inform future putative strategies for pharmacologically targeting PSAT1.

Acknowledgements

Not applicable.

Funding

This study was supported by the Kentucky Lung Cancer Research Program and the Office of the Assistant Secretary of Defense for Health Affairs and the Defense Health Agency J9, Research and Development Directorate, through the Lung Cancer Research Program (grant no. W81XWH-19-1-0445). Sequencing and bioinformatics support for this work was provided by the National Institutes of Health (grant nos. P20GM103436 and P30GM106396).

Availability of data and materials

The data generated in the present study may be found in the GEO database under accession number GSE173270 or at the following URL: https://www.ncbi.nlm.nih.gov/geo/query/acc.cgi?acc=GSE173270.

Authors' contributions

RBS contributed to the conception and design of the study, performed all the *in vitro* studies, the bioinformatics comparative analysis and assisted in writing the manuscript. SW performed the RNA-seq and assisted with the analysis. KA and ER performed the bioinformatics analysis related to the RNA sequencing. BFC contributed to the conception and design of the study, performed the data interpretation and assisted in writing and editing the manuscript. RBS and BFC confirm the authenticity of all the raw data. All authors have read and approved the final manuscript.

Ethics approval and consent to participate

Not applicable.

Patient consent for publication

Not applicable.

Competing interests

The authors declare that they have no competing interests.

References

1. Hanahan D and Weinberg RA: Hallmarks of cancer: The next generation. Cell 144: 646-674, 2011.
2. Zhou X, Tian C, Cao Y, Zhao M and Wang K: The role of serine metabolism in lung cancer: From oncogenesis to tumor treatment. Front Genet 13: 1084609, 2023.
3. Kim SK, Jung WH and Koo JS: Differential expression of enzymes associated with serine/glycine metabolism in different breast cancer subtypes. PLoS One 9: e101004, 2014.
4. Sun WY, Kim HM, Jung WH and Koo JS: Expression of serine/glycine metabolism-related proteins is different according to the thyroid cancer subtype. J Transl Med 14: 168, 2016.
5. Mullarky E, Lucki NC, Beheshti Zavareh R, Anglin JL, Gomes AP, Nicolay BN, Wong JC, Christen S, Takahashi H, Singh PK, *et al*: Identification of a small molecule inhibitor of 3-phosphoglycerate dehydrogenase to target serine biosynthesis in cancers. Proc Natl Acad Sci USA 113: 1778-1783, 2016.
6. Pacold ME, Brimacombe KR, Chan SH, Rohde JM, Lewis CA, Swier LJ, Possemato R, Chen WW, Sullivan LB, Fiske BP, *et al*: A PHGDH inhibitor reveals coordination of serine synthesis and one-carbon unit fate. Nat Chem Biol 12: 452-458, 2016.
7. Zhu S, Wang X, Liu L and Ren G: Stabilization of Notch1 and β-catenin in response to ER-breast cancer-specific up-regulation of PSAT1 mediates distant metastasis. Transl Oncol 20: 101399, 2022.
8. Zhang Y, Li J, Dong X, Meng D, Zhi X, Yuan L and Yao L: PSAT1 regulated oxidation-reduction balance affects the growth and prognosis of epithelial ovarian cancer. Onco Targets Ther 13: 5443-5453, 2020.
9. Fang Y, Liang X, Xu J and Cai X: miR-424 targets AKT3 and PSAT1 and has a tumor-suppressive role in human colorectal cancer. Cancer Manag Res 10: 6537-6547, 2018.
10. Wang H, Cui L, Li D, Fan M, Liu Z, Liu C, Pan S, Zhang L, Zhang H and Zhao Y: Overexpression of PSAT1 regulated by G9A sustains cell proliferation in colorectal cancer. Signal Transduct Target Ther 5: 47, 2020.
11. Biyik-Sit R, Kruer T, Dougherty S, Bradley JA, Wilkey DW, Merchant ML, Trent JO and Clem BF: Nuclear pyruvate kinase M2 (PKM2) contributes to phosphoserine aminotransferase 1 (PSAT1)-mediated cell migration in EGFR-activated lung cancer cells. Cancers (Basel) 13: 3938, 2021.
12. Luo MY, Zhou Y, Gu WM, Wang C, Shen NX, Dong JK, Lei HM, Tang YB, Liang Q, Zou JH, *et al*: Metabolic and nonmetabolic functions of PSAT1 coordinate signaling cascades to confer EGFR inhibitor resistance and drive progression in lung adenocarcinoma. Cancer Res 82: 3516-3531, 2022.
13. Duan W and Liu X: PSAT1 upregulation contributes to cell growth and cisplatin resistance in cervical cancer cells via regulating PI3K/AKT signaling pathway. Ann Clin Lab Sci 50: 512-518, 2020.
14. Gao S, Ge A, Xu S, You Z, Ning S, Zhao Y and Pang D: PSAT1 is regulated by ATF4 and enhances cell proliferation via the GSK3β/β-catenin/cyclin D1 signaling pathway in ER-negative breast cancer. J Exp Clin Cancer Res 36: 179, 2017.
15. Yang Y, Wu J, Cai J, He Z, Yuan J, Zhu X, Li Y, Li M and Guan H: PSAT1 regulates cyclin D1 degradation and sustains proliferation of non-small cell lung cancer cells. Int J Cancer 136: E39-E50, 2015.
16. Wu S and Le H: Dual roles of PKM2 in cancer metabolism. Acta Biochim Biophys Sin (Shanghai) 45: 27-35, 2013.
17. Sutendra G, Kinnaird A, Dromparis P, Paulin R, Stenson TH, Haromy A, Hashimoto K, Zhang N, Flaim E and Michelakis ED: A nuclear pyruvate dehydrogenase complex is important for the generation of acetyl-CoA and histone acetylation. Cell 158: 84-97, 2014.
18. O'Cathail SM, Wu CH, Lewis A, Holmes C, Hawkins MA and Maughan T: NRF2 metagene signature is a novel prognostic biomarker in colorectal cancer. Cancer Genet 248-249: 1-10, 2020.
19. Wang X, Yu Q, Ghareeb WM, Zhang Y, Lu X, Huang Y, Huang S, Sun Y, Lin J, Liu J and Chi P: Downregulated SPINK4 is associated with poor survival in colorectal cancer. BMC Cancer 19: 1258, 2019.
20. You GR, Cheng AJ, Lee LY, Huang YC, Liu H, Chen YJ and Chang JT: Prognostic signature associated with radioresistance in head and neck cancer via transcriptomic and bioinformatic analyses. BMC Cancer 19: 64, 2019.
21. Kim D, Pertea G, Trapnell C, Pimentel H, Kelley R and Salzberg SL: TopHat2: Accurate alignment of transcriptomes in the presence of insertions, deletions and gene fusions. Genome Biol 14: R36, 2013.
22. Trapnell C, Roberts A, Goff L, Pertea G, Kim D, Kelley DR, Pimentel H, Salzberg SL, Rinn JL and Pachter L: Differential gene and transcript expression analysis of RNA-seq experiments with TopHat and cufflinks. Nat Protoc 7: 562-578, 2012.
23. de Hoon MJL, Imoto S, Nolan J and Miyano S: Open source clustering software. Bioinformatics 20: 1453-1454, 2004.

24. Saldanha AJ: Java Treeview-extensible visualization of microarray data. Bioinformatics 20: 3246-3248, 2004.
25. Livak KJ and Schmittgen TD: Analysis of relative gene expression data using real-time quantitative PCR and the 2(-Delta Delta C(T)) method. Methods 25: 402-408, 2001.
26. Simon R, Lam A, Li MC, Ngan M, Menenzes S and Zhao Y: Analysis of gene expression data using BRB-ArrayTools. Cancer Inform 3: 11-17, 2007.
27. Okayama H, Kohno T, Ishii Y, Shimada Y, Shiraishi K, Iwakawa R, Furuta K, Tsuta K, Shibata T, Yamamoto S, *et al*: Identification of genes upregulated in ALK-positive and EGFR/KRAS/ALK-negative lung adenocarcinomas. Cancer Res 72: 100-111, 2012.
28. Simon RM, Subramanian J, Li MC and Menezes S: Using cross-validation to evaluate predictive accuracy of survival risk classifiers based on high-dimensional data. Brief Bioinform 12: 203-214, 2011.
29. Nguyen DX, Chiang AC, Zhang XHF, Kim JY, Kris MG, Ladanyi M, Gerald WL and Massagué J: WNT/TCF signaling through LEF1 and HOXB9 mediates lung adenocarcinoma metastasis. Cell 138: 51-62, 2009.
30. Bair E and Tibshirani R: Semi-supervised methods to predict patient survival from gene expression data. PLoS Biol 2: E108, 2004.
31. Yang W, Xia Y, Ji H, Zheng Y, Liang J, Huang W, Gao X, Aldape K and Lu Z: Nuclear PKM2 regulates β-catenin transactivation upon EGFR activation. Nature 480: 118-122, 2011.
32. Snaebjornsson MT and Schulze A: Non-canonical functions of enzymes facilitate cross-talk between cell metabolic and regulatory pathways. Exp Mol Med 50: 1-16, 2018.
33. Liberzon A, Subramanian A, Pinchback R, Thorvaldsdóttir H, Tamayo P and Mesirov JP: Molecular signatures database (MSigDB) 3.0. Bioinformatics 27: 1739-1740, 2011.
34. Gross SR: Actin binding proteins: Their ups and downs in metastatic life. Cell Adh Migr 7: 199-213, 2013.
35. Beurel E, Grieco SF and Jope RS: Glycogen synthase kinase-3 (GSK3): Regulation, actions, and diseases. Pharmacol Ther 148: 114-131, 2015.
36. Nakata A, Yoshida R, Yamaguchi R, Yamauchi M, Tamada Y, Fujita A, Shimamura T, Imoto S, Higuchi T, Nomura M, *et al*: Elevated β-catenin pathway as a novel target for patients with resistance to EGF receptor targeting drugs. Sci Rep 5: 13076, 2015.
37. Nakayama S, Sng N, Carretero J, Welner R, Hayashi Y, Yamamoto M, Tan AJ, Yamaguchi N, Yasuda H, Li D, *et al*: β-catenin contributes to lung tumor development induced by EGFR mutations. Cancer Res 74: 5891-5902, 2014.
38. Yang F, Li Y, Liu B, You J and Zhou Q: Cancer stem cell-like population is preferentially suppressed by EGFR-TKIs in EGFR-mutated PC-9 tumor models. Exp Cell Res 362: 195-202, 2018.
39. Yang F, Xu J, Li H, Tan M, Xiong X and Sun Y: FBXW2 suppresses migration and invasion of lung cancer cells via promoting β-catenin ubiquitylation and degradation. Nat Commun 10: 1382, 2019.
40. Fan FT, Shen CS, Tao L, Tian C, Liu ZG, Zhu ZJ, Liu YP, Pei CS, Wu HY, Zhang L, *et al*: PKM2 regulates hepatocellular carcinoma cell epithelial-mesenchymal transition and migration upon EGFR activation. Asian Pac J Cancer Prev 15: 1961-1970, 2014.
41. Aktary Z, Bertrand JU and Larue L: The WNT-less wonder: WNT-independent β-catenin signaling. Pigment Cell Melanoma Res 29: 524-540, 2016.
42. Arce L, Yokoyama NN and Waterman ML: Diversity of LEF/TCF action in development and disease. Oncogene 25: 7492-7504, 2006.
43. Robertson H, Hayes JD and Sutherland C: A partnership with the proteasome; the destructive nature of GSK3. Biochem Pharmacol 147: 77-92, 2018.
44. Valenta T, Hausmann G and Basler K: The many faces and functions of β-catenin. EMBO J 31: 2714-2736, 2012.
45. Arao T, Fukumoto H, Takeda M, Tamura T, Saijo N and Nishio K: Small in-frame deletion in the epidermal growth factor receptor as a target for ZD6474. Cancer Res 64: 9101-9104, 2004.
46. Zhou W, Han L and Altman RB: Imputing gene expression to maximize platform compatibility. Bioinformatics 33: 522-528, 2017.
47. Amelio I, Markert EK, Rufini A, Antonov AV, Sayan BS, Tucci P, Agostini M, Mineo TC, Levine AJ and Melino G: p73 regulates serine biosynthesis in cancer. Oncogene 33: 5039-5046, 2014.
48. Chan YC, Chang YC, Chuang HH, Yang YC, Lin YF, Huang MS, Hsiao M, Yang CJ and Hua KT: Overexpression of PSAT1 promotes metastasis of lung adenocarcinoma by suppressing the IRF1-IFNγ axis. Oncogene 39: 2509-2522, 2020.
49. Mattaini KR, Sullivan MR and Vander Heiden MG: The importance of serine metabolism in cancer. J Cell Biol 214: 249-257, 2016.
50. DeNicola GM, Chen PH, Mullarky E, Sudderth JA, Hu Z, Wu D, Tang H, Xie Y, Asara JM, Huffman KE, *et al*: NRF2 regulates serine biosynthesis in non-small cell lung cancer. Nat Genet 47: 1475-1481, 2015.
51. Liu B, Jia Y, Cao Y, Wu S, Jiang H, Sun X, Ma J, Yin X, Mao A and Shang M: Overexpression of phosphoserine aminotransferase 1 (PSAT1) predicts poor prognosis and associates with tumor progression in human esophageal squamous cell carcinoma. Cell Physiol Biochem 39: 395-406, 2016.
52. Morita T, Mayanagi T and Sobue K: Reorganization of the actin cytoskeleton via transcriptional regulation of cytoskeletal/focal adhesion genes by myocardin-related transcription factors (MRTFs/MAL/MKLs). Exp Cell Res 313: 3432-3445, 2007.
53. Gau D and Roy P: SRF'ing and SAP'ing-the role of MRTF proteins in cell migration. J Cell Sci 131: jcs218222, 2018.
54. Shi X, Zhao S, Cai J, Wong G and Jiu Y: Active FHOD1 promotes the formation of functional actin stress fibers. Biochem J 476: 2953-2963, 2019.
55. Schönichen A, Mannherz HG, Behrmann E, Mazur AJ, Kühn S, Silván U, Schoenenberger CA, Fackler OT, Raunser S, Dehmelt L and Geyer M: FHOD1 is a combined actin filament capping and bundling factor that selectively associates with actin arcs and stress fibers. J Cell Sci 126: 1891-1901, 2013.
56. Heuser VD, Mansuri N, Mogg J, Kurki S, Repo H, Kronqvist P, Carpén O and Gardberg M: Formin proteins FHOD1 and INF2 in triple-negative breast cancer: Association with basal markers and functional activities. Breast Cancer (Auckl) 12: 1178223418792247, 2018.
57. Gardberg M, Kaipio K, Lehtinen L, Mikkonen P, Heuser VD, Talvinen K, Iljin K, Kampf C, Uhlen M, Grénman R, *et al*: FHOD1, a formin upregulated in epithelial-mesenchymal transition, participates in cancer cell migration and invasion. PLoS One 8: e74923, 2013.
58. Koka S, Neudauer CL, Li X, Lewis RE, McCarthy JB and Westendorf JJ: The formin-homology-domain-containing protein FHOD1 enhances cell migration. J Cell Sci 116: 1745-1755, 2003.
59. Rottner K, Faix J, Bogdan S, Linder S and Kerkhoff E: Actin assembly mechanisms at a glance. J Cell Sci 130: 3427-3435, 2017.
60. Lee CW, Vitriol EA, Shim S, Wise AL, Velayutham RP and Zheng JQ: Dynamic localization of G-actin during membrane protrusion in neuronal motility. Curr Biol 23: 1046-1056, 2013.
61. Ji P, Diederichs S, Wang W, Böing S, Metzger R, Schneider PM, Tidow N, Brandt B, Buerger H, Bulk E, *et al*: MALAT-1, a novel noncoding RNA, and thymosin beta4 predict metastasis and survival in early-stage non-small cell lung cancer. Oncogene 22: 8031-8041, 2003.
62. Fei F, Qu J, Zhang M, Li Y and Zhang S: S100A4 in cancer progression and metastasis: A systematic review. Oncotarget 8: 73219-73239, 2017.
63. Peippo M, Gardberg M, Lamminen T, Kaipio K, Carpén O and Heuser VD: FHOD1 formin is upregulated in melanomas and modifies proliferation and tumor growth. Exp Cell Res 350: 267-278, 2017.
64. Morita T and Hayashi K: Tumor progression is mediated by thymosin-β4 through a TGFβ/MRTF signaling axis. Mol Cancer Res 16: 880-893, 2018.
65. Morita T and Hayashi K: G-actin sequestering protein thymosin-β4 regulates the activity of myocardin-related transcription factor. Biochem Biophys Res Commun 437: 331-335, 2013.
66. da Cunha BR, Domingos C, Stefanini ACB, Henrique T, Polachini GM, Castelo-Branco P and Tajara EH: Cellular interactions in the tumor microenvironment: The role of secretome. J Cancer 10: 4574-4587, 2019.
67. Karagiannis GS, Pavlou MP and Diamandis EP: Cancer secretomics reveal pathophysiological pathways in cancer molecular oncology. Mol Oncol 4: 496-510, 2010.
68. Lin A, Wei T, Meng H, Luo P and Zhang J: Role of the dynamic tumor microenvironment in controversies regarding immune checkpoint inhibitors for the treatment of non-small cell lung cancer (NSCLC) with EGFR mutations. Mol Cancer 18: 139, 2019.

69. Li H, Wu C, Chang W, Zhong L, Gao W, Zeng M, Wen Z, Mai S and Chen Y: Overexpression of PSAT1 is correlated with poor prognosis and immune infiltration in non-small cell lung cancer. Front Biosci (Landmark Ed) 28: 243, 2023.
70. Sivanand S, Rhoades S, Jiang Q, Lee JV, Benci J, Zhang J, Yuan S, Viney I, Zhao S, Carrer A, *et al*: Nuclear Acetyl-CoA production by ACLY promotes homologous recombination. Mol Cell 67: 252-265.e6, 2017.
71. Wang Y, Guo YR, Liu K, Yin Z, Liu R, Xia Y, Tan L, Yang P, Lee JH, Li XJ, *et al*: KAT2A coupled with the α-KGDH complex acts as a histone H3 succinyltransferase. Nature 552: 273-277, 2017.
72. Kottakis F, Nicolay BN, Roumane A, Karnik R, Gu H, Nagle JM, Boukhali M, Hayward MC, Li YY, Chen T, *et al*: LKB1 loss links serine metabolism to DNA methylation and tumorigenesis. Nature 539: 390-395, 2016.
73. Hwang IY, Kwak S, Lee S, Kim H, Lee SE, Kim JH, Kim YA, Jeon YK, Chung DH, Jin X, *et al*: Psat1-dependent fluctuations in α-ketoglutarate affect the timing of ESC differentiation. Cell Metab 24: 494-501, 2016.
74. Harmston N and Lenhard B: Chromatin and epigenetic features of long-range gene regulation. Nucleic Acids Res 41: 7185-7199, 2013.
75. Clark SJ: Action at a distance: Epigenetic silencing of large chromosomal regions in carcinogenesis. Hum Mol Genet 16 Spec No 1: R88-R95, 2007.
76. Ahn MJ, Won HH, Lee J, Lee ST, Sun JM, Park YH, Ahn JS, Kwon OJ, Kim H, Shim YM, *et al*: The 18p11.22 locus is associated with never smoker non-small cell lung cancer susceptibility in Korean populations. Hum Genet 131: 365-372, 2012.